

Size Independent Shape Memory Behavior of Nickel–Titanium**

By Blythe G. Clark*, Daniel S. Gianola, Oliver Kraft and Carl P. Frick

While shape memory alloys such as NiTi have strong potential as active materials in many small-scale applications, much is still unknown about their shape memory and deformation behavior as size scale is reduced. This paper reports on two sets of experiments which shed light onto an inconsistent body of research regarding the behavior of NiTi at the nano- to microscale. In situ SEM pillar bending experiments directly show that the shape memory behavior of NiTi is still present for pillar diameters as small as 200 nm. Uniaxial pillar compression experiments demonstrate that plasticity of the phase transformation in NiTi is size independent and, in contrast to bulk single crystal observations, is not influenced by heat treatment (i.e., precipitate structure).

Shape memory alloys represent a class of so-called “smart” materials that can be returned to their original shape after deformation, either spontaneously or through the application of heat. While several alloys are capable of shape memory

behavior, nickel–titanium (NiTi) is the most extensively researched due primarily to its relatively large deformation recoverability,^[1] as well as its high strength,^[2] corrosion resistance,^[3] biocompatibility,^[4] and high intrinsic damping.^[5] The shape memory effect for NiTi results from a reversible martensitic phase transformation, in which the crystal structure shifts from a B2 (austenite) to a B19' (martensite) phase in a shear-like manner. Depending upon composition and processing history, the stress-induced martensitic phase transformation is capable of two responses: pseudoelasticity and shape memory behavior. Pseudoelasticity occurs when the martensite is unstable at the testing temperature and spontaneously reverts back to austenite upon unloading, recovering the previously accumulated deformation. Shape memory behavior occurs when the martensite is stable at the testing temperature, requiring heat to revert to austenite and recover the strain associated with the phase transformation.

Monotonic uniaxial stress–strain testing of shape memory NiTi is well-known to exhibit four stages of deformation, each dominated by a specific mechanism as a function of increasing strain: (I) elastic deformation of austenite, (II) austenite-to-martensite phase transformation, (III) elastic deformation of martensite, and (IV) martensite plasticity.^[6] The martensite phase transformation is exemplified by a critical stress at which the phase transformation initiates, followed by a decrease in stress/strain slope signifying the propagation of the martensite throughout the sample.^[1] Nominal values of the critical martensite initiation stress, transformation slope, and transformation strain are heavily influenced by processing history, microstructure, and crystallographic orientation. Because the phase transformation is temperature dependent,

[*] Dr. B. G. Clark^[+]

Max Planck Institute for Metals Research, Heisenbergstrasse
3 70569 Stuttgart, Germany

INM-Leibniz Institute for New Materials, Campus Building
D2 2, 66123 Saarbrücken, Germany

Prof. D. S. Gianola^[++], Prof. O. Kraft

Karlsruhe Institute of Technology, Institute for Materials
Research II,

Postfach 3640, D-76021 Karlsruhe, Germany

Prof. C. P. Frick

Department of Mechanical Engineering, University of
Wyoming, Department 3295, 1000 E. University Ave,

Laramie, WY 82071, USA

E-mail: cfcrick@uwyo.edu

[+] Current address: Sandia National Laboratories, Physical,
Chemical, and Nano Sciences Center, PO Box 5800, MS
1423 Albuquerque, NM, 87185, USA

[++] Current address: Department of Materials Science and
Engineering, University of Pennsylvania, 205 LRSM, 3231
Walnut Street, Philadelphia, PA 19104, USA

[**] Acknowledgements, The authors would like to acknowledge the assistance of Ulrike Eigenthaler and Dr. Michael Hirscher with the DualBeamTM, FIB Additionally we would like to thank Dr. Yuri Chumlyakov of the Siberian Physical Technical Institute for creating the single crystal NiTi samples. B. G. C. and D. S. G. would like to acknowledge funding from Alexander von Humboldt Fellowships.

stress-induced martensite will revert to austenite upon heating above the austenite finish temperature (A_f), while plastic deformation induced in the martensite phase will remain permanent.

Because the actuation mechanism is inherent to the material, NiTi is of particular interest for small-scale applications^[7] and is often proposed as the active material in functional devices.^[8] This feature has been exploited in micro-electrical-mechanical systems (MEMS),^[9] as NiTi has been shown to have a higher work output per unit volume than any conventional actuator.^[10] Although understanding the mechanical behavior of NiTi at small-scales is crucial to such applications, it remains unclear how size scale influences the shape memory effect; to date, investigations into the size dependency of the NiTi martensitic phase transformation have yielded contradictory results.^[11–17] Similarly, many unanswered questions remain concerning the influence of sample size on martensite plasticity. To shed light on these areas, this study investigates the size effect on shape memory behavior and plasticity in focused ion beam (FIB) machined NiTi pillars that were aged to elicit shape memory behavior at room temperature.^[18] To study the influence of size on shape memory effect, pillars $\approx 1\ \mu\text{m}$ and 200 nm in diameter were subjected to bending via angled application of load during *in situ* scanning electron microscope (SEM) observation. After subsequent *ex situ* heating, all pillars showed partial to full recovery, clearly demonstrating deformation recovery regardless of sample size. To study the size effect on plasticity, uniaxial compression experiments on similar size pillars were conducted using a nanoindenter equipped with a flat punch. The results indicate that plasticity of martensite is independent of sample size or precipitate structure, which is corroborated by previous work of the same authors.^[19–21]

Experimental

With exception to the specific aging temperature, preparation of NiTi compression pillars was nearly identical to the process used in previous studies.^[20,21] Nominally Ti-50.9 at% Ni single crystal was solutionized, and subsequently aged at 450 °C for 1.5 h followed by a water quench. This heat treatment was explicitly used to form Ti_3Ni_4 precipitates $\approx 50\ \text{nm}$ in diameter. The relatively large internal stress caused by the semi-coherent interface of the precipitates is known to assist in phase transformation,^[22] resulting in shape memory behavior at room temperature.^[23] Bulk Ti-50.9 at% Ni given an identical aging treatment had austenite start (A_s) and finish (A_f) temperatures of 25 and 33 °C, respectively.^[18] A $\approx 4\ \text{mm} \times 4\ \text{mm} \times 7\ \text{mm}$ NiTi specimen oriented such that the long direction was

aligned with the [111] crystallographic direction was electro-discharge machined. The sample surface was mechanically polished under low force (approximately one pound) with decreasing grit size, ending with a 0.25 μm diamond solution. In order to remove the surface layer affected by mechanical polishing, the specimen was then electropolished at 15 V for 2.5 min in a 5% perchloric acid, 95% ethanol solution. Free-standing compression pillars with diameters ranging from $\approx 2\ \mu\text{m}$ to below 200 nm were FIB machined into the electropolished surface. All FIB cuts were made using a voltage of 30 kV, at currents ranging from 7 nA for rough cuts, down to 10 pA for the final cuts. Because all pillars were created using top-down annular FIB milling, all pillars had an estimated taper angle of $\approx 3^\circ\text{--}5^\circ$, which is similar to other micro-pillar studies using the same basic manufacturing technique.^[24]

The *in situ* SEM pillar bending setup used is shown in Figure 1. Pillars were fabricated on the electropolished top edge to assist in lateral SEM imaging. *In situ* bending was performed using a flat diamond punch tip oriented at an angle relative to the long axis of the pillar [Fig. 1(b)]. Because each free-standing pillar was produced by removal of surrounding material, essentially creating a circular trough, angles ranging from 40° to 60° were chosen to ensure that the indenter only contacted the pillar and did not come in contact with the trough sidewall. Bending was selected as the mode of deformation due to the large tip deflections that can be achieved (i.e., large lateral compliance), facilitating the observation of relative changes in specimen shape due to plastic deformation and shape recovery. The transducer was operated in feedback-enabled displacement control, which provided stable incremental deformation, avoided large strain bursts, and provided a real-time output of the load and displacement applied on the specimens. The displacement rate for testing was 0.5 nm s^{-1} for the small ($\approx 200\ \text{nm}$ diameter) and 1 nm s^{-1} for the large ($\approx 1\ \mu\text{m}$) pillars. SEM images were captured during bending to visualize the

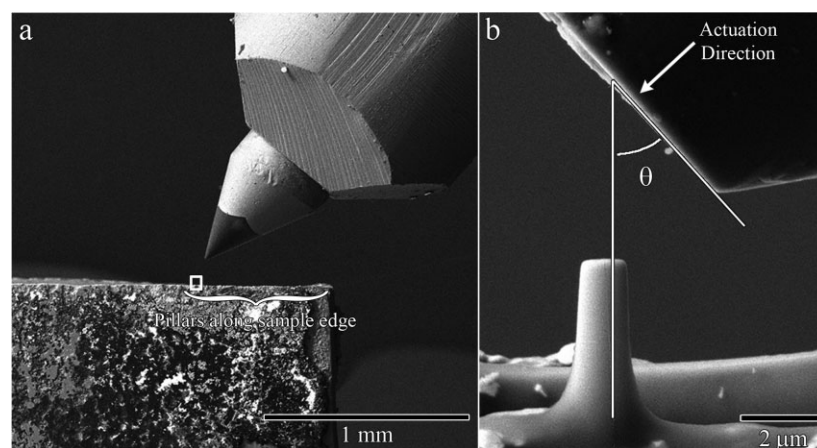


Fig. 1. SEM images of the *in situ* bending setup used for pillar bending. (a) Edge-on view of the [111] NiTi sample and the flat conductive diamond punch tip, and (b) higher magnification view showing the orientation of the flat punch with respect to the NiTi pillars (θ was in the range of 40°–60° for all tests). The small box drawn in (a) indicates the location and area of the image in (b).

deformation and to correlate the load–displacement curve to testing events. After bending, pillars were heated *ex situ* at 200 °C for 5 min to elicit phase transformation deformation recovery, and reimaged with the SEM.

Due to the inherent pillar taper, the angle of applied force, indenter/pillar slipping, and unknown constitutive response (nonlinear relationship between stress and strain) a quantitative transformation of the force–displacement data to stress–strain values was not attempted. Furthermore, while displacement and force resolution were adequate for the pillars tested near 1 μm in diameter, significant noise was observed for pillars 200 nm in diameter. Therefore, digital image correlation (DIC) software^[25] was used to measure the strain evolution on the pillar surface from SEM images obtained during *in situ* bending experiments. DIC relies on the correlation of the intensity distribution of small subsets of pixels between a reference and a deformed digital image, providing displacement fields. Quasi-full-field strains can be computed from the gradients of the displacement fields with respect to spatial position, requiring no recourse to a model of constitutive behavior for strain measurement. Custom MATLAB-based scripts^[25] were employed for the calculations reported here. Strain analysis was performed for the two larger pillars deformed via *in situ* bending, but a lack of contrast and poor signal-to-noise ratio in the images of the small pillars precluded an accurate strain measurement in those cases. Nevertheless, estimates of strain recovery for all pillars were obtained by quantifying tip displacement vectors from the *in situ* post-heated digital images. Vectors were computed by measuring the distance between a high-contrast point on the pillar tips in the undeformed, post-deformed, and post-heated overlaid SEM images. The amount of recovery is calculated as percent difference between the magnitude of the displacement vectors of the post-bending and post-heating states. This was performed for several points on the pillar tips to estimate error, which was computed to be less than 5%. It is important to note that [111] NiTi is well known to exhibit an asymmetrical tension/compression response. Therefore strain values measured from image correlation were always taken from the compression-side, to allow for relative comparison to pillar compression testing.

Compression tests were conducted with a nanoindenter system operated in load-control, equipped with a sapphire conical indenter with a flat 10 μm diameter tip. Loading rates varied with sample length such that the approximate testing time ranged between 3 and 5 min. The martensitic phase transformation occurs at a rate on the order of dislocation velocities, therefore it is not expected that significant time-dependent deformation occurred over this time scale. Pillars were imaged pre- and post-testing using SEM. In consideration of the slight pillar taper, engineering stress was calculated using the pillar top diameter. This was done because the top is straightforward to define and plasticity was often observed toward the top half of the pillar. It is recognized that this is a maximum estimate of stress, which will vary ≈50% across the length of the pillar.^[26]

Results and Discussion

Size Effect on Shape Memory Behavior

Frick *et al.* investigated the size dependence of the martensitic phase transformation via compression of FIB-machined [111] NiTi pillars heat treated to produce pseudoelastic behavior.^[20,21] Results showed that NiTi pillars with diameters ranging from ≈2 μm to 400 nm exhibited pseudoelasticity and bulk-like behavior. However, as diameter was decreased, pseudoelasticity (evidenced by hysteresis during unloading) was subdued for diameters of 400–200 nm, and fully inhibited for diameters of ≈200 nm or below. Overall these observations were extremely robust, with phase transformation recovery being inhibited at diameters less than 200 nm for multiple single crystal orientations and precipitate sizes. It was hypothesized that either the martensitic phase transformation had been suppressed for the smallest pillars, or the phase transformation had occurred but the strain recovery had been inhibited. In a recent investigation by Ye *et al.*, 200 nm diameter pseudoelastic NiTi pillars were manufactured and compressed in a similar manner during *in situ* transmission electron microscope (TEM) observation.^[27] Based on electron diffraction information, they concluded that the martensitic phase transformation is still active in NiTi at small size scales. However their pseudoelastic behavior was difficult to interpret due to recoverable deformation beneath the pillar, likely due to their two-tiered geometry created during FIB machining. Regardless, direct observation of the martensitic phase for their 200 nm pillars suggests that the suppression of pseudoelasticity observed previously^[20,21] can be explained by a suppression of strain recovery, not that of the martensitic phase transformation. Although the mechanism for suppression of strain recovery remains unclear, one possible explanation may be the mechanical influence of the Ga⁺ ion damaged surface layer. FIB milling is known to induce an amorphous Ga⁺ ion embedded damage layer ≈10–20 nm in depth for an angle of incidence close to 90°. ^[20] For a 200 nm diameter pillar, the damage layer is estimated to be ≈10–20% of the total cross-section. Thus it is possible that the FIB damage layer produces a mechanical barrier, becoming more significant with decrease in diameter and inhibiting reverse phase transformation for pseudoelastic material upon unloading. However, the mechanical properties of the damaged layer are unknown, thus inhibiting a quantitative analysis of the above scenario not possible. The possibility also exists that as pillar diameter approaches the size of the martensitic plates, the martensitic phase may remain stable post-deformation. However, this possibility seems unlikely as TEM images observe martensitic plates approximately 15–30 nm in width. A free energy analysis of the phase transformation behavior as a function of size-scale is beyond the scope of this work.

In order to better understand the recoverability of the phase transformation in NiTi as a function of sample size and strain, *in situ* SEM bending experiments followed by subsequent heating were chosen for this study, similar to

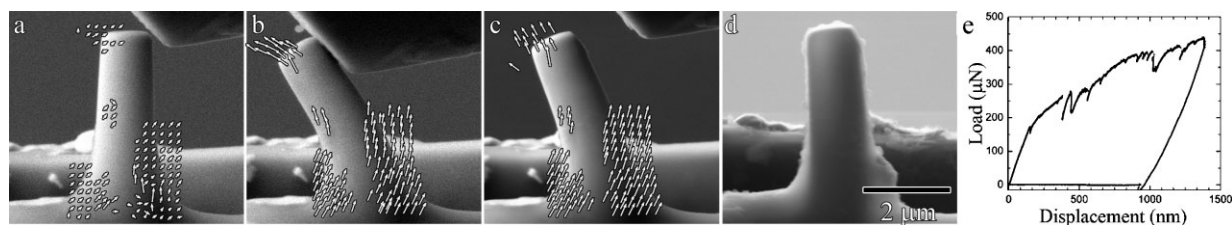


Fig. 2. SEM images showing a representative experimental sequence. (a) Initial configuration of a 1.2 μm [111] NiTi pillar and angled flat-tip punch pre-testing, (b) *in situ* bending of the pillar via angled application of load, shown at the point of maximum bending, (c) shape of the NiTi pillar after release of load, showing significant residual deformation (maximum strain = 9%), and (d) pillar after *ex situ* heating at 200 °C for 5 min, showing near complete shape recovery. Shown in (e) is the corresponding load–displacement curve for (a–c). White arrows in (a–c) are displacement vectors at various points along the pillar surface produced from digital image correlation. The displacement field gradients are used to derive strains. See text for details.

testing performed on Cu–Al–Ni shape memory alloys.^[28] The setup for the *in situ* SEM bending experiments is shown in Figure 1. The cantilever geometry of the pillar allowed for large tip displacements enabling facile imaging of deformation and recovery. In addition, any compliance effects of the material beneath the pillar are expected to be minimal since the deformation is relatively localized in bending. In Figure 2, a representative *in situ* bending actuation sequence for a 1.2 μm diameter [111] NiTi pillar is shown. The SEM images in Figure 2(a–d) show, respectively: the initial pillar configuration pre-testing, maximum bending via angled application of load, residual deformation after release of load, and the pillar after *ex situ* heating to 200 °C for 5 min demonstrating partial deformation recovery. For NiTi of the same composition and heat treatment as that used in this study, A_f was measured to be 33 °C.^[18] Thus, the observed behavior is consistent with expectation: heating the pillars to 200 °C for 5 min should recover deformation associated with the phase transformation, while plastic deformation should remain. White arrows in Figure 2(a–c) represent displacement vectors of various points on the pillar as computed by DIC of the *in situ* image sequences.^[25] Details can be found in the Experimental section. For the representative 1.2 μm pillar shown in Figure 2, the maximum compressive strain resulting from bending was nearly 9% while a residual strain of $\approx 4\%$ remained upon unloading.

The corresponding load–displacement data for the 1.2 μm diameter pillar [Fig. 2(e)] demonstrates elastic loading followed by a deviation from linearity, consistent with the residual deformation (bent shape) of the pillar observed in Figure 2(c). The actuation direction is normal to the face of the indenter, therefore pillars were subjected to transverse and axial loads during deformation. However, several load drops are observed during actuation, which were found to correspond to discrete slipping events between the indenter and the pillar. This observation of sliding suggests that the

stresses are incurred predominately from the transverse component of the load. The load–displacement behavior in Figure 2(e) does not exhibit all four stages of deformation expected for uniaxial loading, despite residual deformation after heating [Fig. 2(d)] which indicates that the fourth deformation stage of martensite plasticity was reached. However, it is important to note that bending elicits a stress gradient through the cross-section of the pillar, likely activating multiple deformation mechanisms at once.

Figure 3 shows all four pillars tested via *in situ* SEM bending. Two pillars with relatively large diameters [900 nm—Fig. 3(a), and 1.2 μm —Fig. 3(b)], and two smaller pillars [300 nm—Fig. 3(c), and 200 nm—Fig. 3(d)] were chosen for testing. Each image in Figure 3 contains three SEM images overlaid on top of one another, such that relative pillar shapes during the progression of deformation steps can be

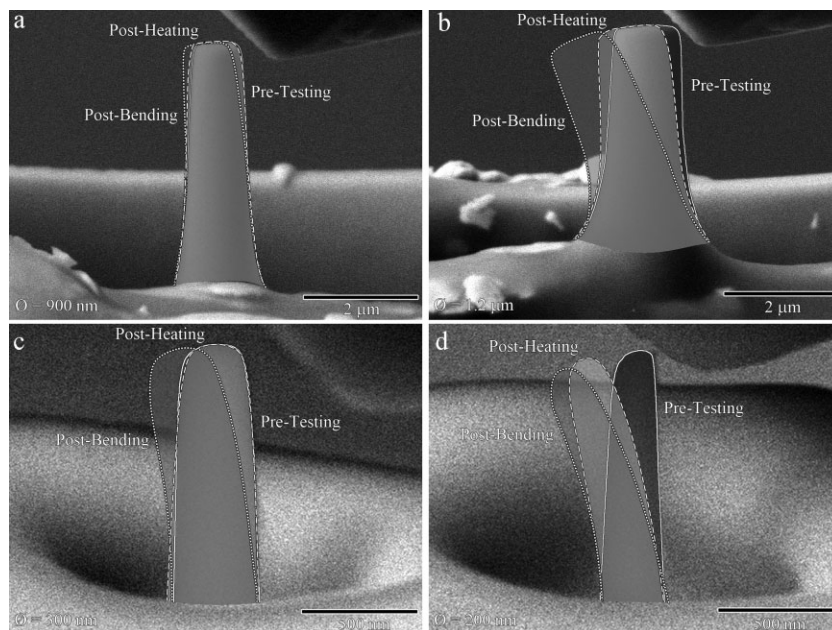


Fig. 3. SEM images overlaid with traces of NiTi pillar shapes pre-testing (solid line), post-bending (dotted line), and post-heating (dashed line) to illustrate shape recovery observed for an (a) 900 nm, (b) 1.2 μm , (c) 300 nm, and (d) 200 nm pillar. Pillars shown in (a) and (c) were bent to small total displacements and show complete shape recovery, while pillars in (b) and (d) were bent to larger total displacements and show partial shape recovery with some residual deformation. Maximum strains of 3 and 9% were calculated for (a) and (b), respectively, using digital image correlation. See text for details.

readily compared. Traces of NiTi pillar shapes pre-testing (solid line), post-bending (dotted line), and post-heating (dashed line) are used to illustrate pillar shape at each step. In summary, the 900 nm pillar shown in Figure 3(a) loaded to a maximum strain of 3% illustrated $\approx 90\%$ recovery. In contrast, the 1.2 μm diameter pillar shown in Figure 3(b) was bent to a larger degree, resulting in a maximum bending strain of $\approx 9\%$. Upon heating, the shape memory deformation was partially recovered, although $\approx 4\%$ residual strain remained. Similar behavior was observed for the 300 and 200 nm pillars shown in Figure 3(c) and (d), respectively. The 300 nm pillar showed nearly 100% recovery after being bent to a small displacement while the 200 nm bent to a larger total displacement recovered only about 30% of the total applied deformation.

Based on the results shown in Figure 3 and recovery measurements, full deformation recovery is possible as long as the imposed mechanical strains are kept low enough as to avoid plasticity of the martensite. Nominal recovery values are similar to those shown in bulk studies.^[2] Results clearly demonstrate that the underlying deformation mechanisms remain relatively unchanged over the size scales tested; the recovery behavior provides direct evidence that [stress-induced] martensite is induced and remains stable, and is therefore not fundamentally inhibited, at this size scale.

Unfortunately, the size independent shape memory results shown in Figure 3 cannot explain the observed size dependent suppression of pseudoelasticity.^[20,21] However, a scenario exists where the damaged surface layer estimated to be 10–20 nm in depth may be strong enough to inhibit pseudoelastic recovery, but too weak to suppress shape memory recovery. Intuitively, this explanation is plausible, as bulk testing of pseudoelastic NiTi demonstrates a relatively low stress at which pseudoelastic recovery occurs,^[2] however, forces generated during shape memory recovery are known to be quite large.^[10] However, no quantitative attempt was made to analyze this possibility, due to the complications of the unknown mechanical behavior of the damaged surface layer, the tapered geometry of the pillars, and the bending loading mode. Therefore, further testing is required to substantiate this theory. Additionally the possibility certainly exists at the scale may have a critical influence on the nature of the martensitic phase transformation, as discussed in the next section.

Size Effect on Plasticity of Martensite

To further understand the deformation of NiTi, especially with respect to the transition from phase transformation deformation to martensite plasticity, additional pillar experiments of uniaxial compression to high strains were conducted. Whereas similar testing of conventional single-crystal metals has shown

that strength scales with decreasing diameter,^[24,29–32] in compression testing of NiTi no strong size effect has been observed.^[21] In contrast to conventional metals, mechanical deformation of NiTi involves a complex interplay between martensitic phase transformation and plasticity. The relatively large local stresses thought to occur at the austenite–martensite interfaces are believed to generate dislocations, observed in cyclically-loaded single crystal studies for both bulk^[33] and micropillar^[34] specimens. A technique often employed to inhibit cyclic degradation is aging to elicit semi-coherent Ti_3Ni_4 precipitates, whose internal stress acts to both limit dislocation motion while promoting the phase transformation.^[18,22,35] Consequently, in Frick *et al.*^[21] the absence of a size effect in the flow stress of martensite was believed to be due to the influence of dislocation obstacles within the microstructure with spacing smaller than the pillar diameter. In NiTi, the martensite is known to take the form of a twinned structure on the order of tens of nanometers,^[22,35,36] and the NiTi tested in Frick *et al.*^[21] contained finely dispersed Ti_3Ni_4 precipitates ≈ 10 nm in size.

In order to better understand the influence of precipitates on the martensite plasticity, the nickel-rich bulk sample used for this study was aged prior to FIB pillar manufacture, to form Ti_3Ni_4 precipitates ≈ 50 nm in diameter.^[23] The results of representative *ex situ* compression tests performed using a conventional force-controlled nanoindenter followed by post-compression SEM imaging are shown in Figure 4. Each sample was loaded to a maximum nominal strain value of 15 to 25% under load control, with two intermediate unloading cycles at ≈ 3 and 5% strain. The maximum strain values were chosen to be past the point of the martensite phase

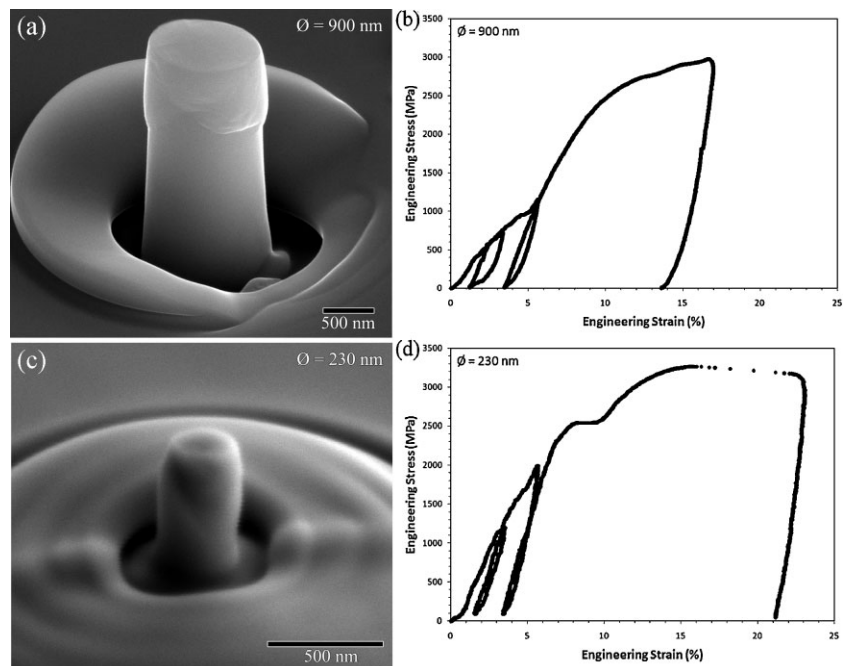


Fig. 4. SEM images and corresponding engineering stress–strain curves for (a, b) a 900 nm pillar and (c, d) a 230 nm [111] NiTi pillar. Stresses were calculated using the top diameter of the pillar.

transformation, and to the point of dislocation motion in the martensite. The initial stress–strain behavior of a 900 nm diameter [Fig. 4(b)] and a 230 nm pillar [Fig. 4(d)] are relatively similar. Each pillar exhibits a relatively low stiffness during initial loading. This has been observed in other micro/nano pillar studies and has been attributed to surface roughness as well as to the small misalignment between pillar and indenter.^[24] In both cases, as nominal strain approaches 1% the stiffness dramatically increases (stage I). As strain increases to $\approx 2\%$ strain, the slope begins to decrease, which is an indication that the martensitic phase transformation has been nucleated and has begun propagating through the pillar (stage II). Because the phase transformation is not crystallographically favored in the compressive [111] direction relative to other orientations (e.g., [210]),^[20] the pillar does not have a distinct critical transformation stress, and the transformation behavior exhibits significant apparent strain hardening, similar to bulk.

Unloading at 3% strain exhibits a much larger stiffness than observed upon initial loading, however, in-depth analysis of nominal values is considered inappropriate because it is likely that the transformation is incomplete. Furthermore, modulus calculations of pillars have been shown to have significant variation between samples due to the non-uniform stress as a result of pillar taper,^[30] and possible non-elastic deformation beneath the pillar.^[27] Elastic modulus estimates vary significantly between the samples tested here, but never reach the value of 47 GPa that has been observed in bulk $\langle 111 \rangle$ textured NiTi with the same heat treatment.^[18] It is also important to note that unloading in Figure 4(b) is nonlinear, and the unloading/loading curves exhibit small hysteresis. Hysteresis is an indication that the martensite is reverting back to austenite spontaneously upon the removal of stress, a signature of a pseudoelastic response. However, the magnitude of strain recovery and the size of the hysteresis envelope is qualitatively well below that observed typically in pseudoelastic pillars of similar size.^[20,21] Because the A_s and A_f transformation temperatures are close to the testing temperature,^[18] it is likely that the NiTi experiences a mixture between pseudoelastic and shape memory response. The example shown in Figure 4(b) represents the most extreme case, with most pillars exhibiting much smaller hysteresis.

Upon further loading the deformation becomes increasingly dominated by elastic behavior of martensite (stage III), although not completely. At relatively high strains ($>10\%$), dislocation motion within the martensite crystal structure causes a substantial deviation from linear elasticity (stage IV). SEM micrographs shown in Figure 4(a) and (c) demonstrate slip traces on the sample surface. This behavior is relatively consistent with recent compression pillar post mortem^[19] and *in situ* TEM^[27] results, which demonstrate dislocation motion in stress-induced martensite. The residual plastic strain measured from pillar compression is in accordance with the *in situ* bending results, where full recovery was not observed if the maximum strain incurred during bending was $\approx 9\%$. This degree of deformation is approximately the transition from

elastic to plastic deformation of the martensite (stage III to stage IV) measured in compression of the 900 nm pillar [Fig. 4(b)].

To quantify the effect of pillar size on martensite plasticity, the stress values at 10% strain as a function of pillar diameter for [111] NiTi aged at 450 °C are plotted in Figure 5. Stress at 10% strain was chosen because all pillars deformed to 10% strain or above exhibited slip events on the pillar surface, and this is well above the strain required for martensite plasticity of aged [111] bulk NiTi compression samples.^[2] For comparison purposes, stress values taken from [111] NiTi pillars aged at 350 °C,^[21] as well as pure [111] Ni pillars,^[30] are also included in Figure 5. The two NiTi samples were cut from the same parent single crystal, and differ only in aging temperature. Both materials are believed to contain evenly distributed Ti_3Ni_4 precipitates, with approximate sizes of 10 and 50 nm for the 350 and 450 °C heat treatments, respectively.^[18] The [111] Ni sample is of high purity, containing no secondary structure, and shows size effect behavior (i.e., increase in strength with decrease in diameter) typical of single crystal metals. Both NiTi heat treatments do not demonstrate a size effect, but rather exhibit a relatively constant martensite strength value regardless of diameter. The 350 °C aged NiTi pillars give an average stress value of 2860 MPa with a standard deviation of 380 MPa. The 450 °C aged pillars have a similar average stress value of 2934 MPa, with a larger standard deviation of 632 MPa.

Compression testing of the NiTi pillars in this study demonstrates size independent martensite yielding. Similar results have been observed for materials with internal obstacle spacing significantly smaller than pillar diameter.^[37] Surprisingly, martensite yield strength was comparable to [111] NiTi pillars with a much smaller precipitate structure, inconsistent with previous micro^[18] and nanoindentation^[17] studies. Comparison of current results with previous results^[20] indicates that in contrast to bulk, martensite plasticity in small-scale pillars is highly dependent on crystal orientation rather than precipitate structure. This indicates that the flow

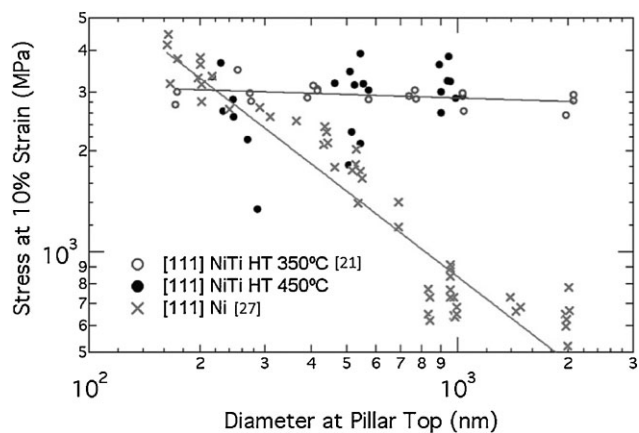


Fig. 5. Comparison of the size effect in [111] Ni pillars to the size-independent behavior of [111] NiTi pillars subjected to different heat treatments (HT). Stress at 10% strain is plotted versus pillar diameter.

stress is driven by a fundamental interaction between the martensitic phase transformation and the dislocation behavior; although further testing is required to better understand this phenomenon.

Conclusions

In summary, *in situ* SEM bending experiments and uniaxial compression experiments were performed on [111] NiTi nano- and micro-pillars aged to induce shape memory behavior at room temperature. Both bending and compressive testing results of NiTi pillars were consistent with the occurrence and stability of martensite phase transformation and shape memory behavior. Bending results showed full recovery for pillars deformed to low maximum strain ($\approx 3\%$), convincingly demonstrating that the recoverable martensitic phase transformation in NiTi occurs for pillars as small as 200 nm in diameter. This indicates that loss of pseudoelasticity in small NiTi pillars^[21] is not reflective of martensite inhibition. Bending of pillars to larger strains ($\approx 9\%$) resulted in partial recovery with some permanent deformation. It is argued that this non-recoverable strain is related to martensite plasticity, which was also found in the uniaxial compression test in this strain regime. However, a significant portion of the deformation was recovered upon heating, indicating that increased dislocation density is not significant enough to inhibit martensitic recovery. For uniaxial compression experiments, stress-strain behavior showed Stage I-IV deformation for all pillars tested, indicating that deformation mechanisms over this size scale is similar to bulk. For strains above 10%, deformation was dominated by martensite plasticity. No size effect for dislocation motion in martensite and no influence of precipitate size was observed. In addition, martensite flow stress remained stable at ≈ 3 GPa regardless of heat treatment, which is consistent with previous pillar results^[19] confirming that martensite plasticity for small-scale pillars is highly dependent on crystal orientation rather than on precipitate structure, sample size, or deformation mode.

Received: January 27, 2010
Final Version: April 6, 2010

- [1] J. A. Shaw, S. Kyriakides, *J. Mech. Phys. Solids* **1995**, *43*, 1243.
- [2] H. Sehitoglu, I. Karaman, R. Anderson, X. Zhang, K. Gall, H. J. Maier, Y. Chumlyakov, *Acta Mater.* **2001**, *49*, 747.
- [3] D. J. Wever, A. G. Veldhuizen, J. de Vries, H. J. Busscher, D. R. A. Uges, J. R. van Horn, *Biomaterials* **1998**, *19*, 761.
- [4] L. Ponsonnet, D. Treheux, M. Lissac, N. Jaffrezic, B. Grosgeat, *Int. J. Appl. Electromagn. Mech.* **2006**, *23*, 147.
- [5] S. Saadat, J. Salichs, M. Noori, Z. Hou, H. Davoodi, I. Bar-On, Y. Suzuki, A. Masuda, *Smart Mater. Struct.* **2002**, *11*, 218.
- [6] K. Gall, J. Tyber, V. Brice, C. P. Frick, H. J. Maier, N. Morgan, *J. Biomed. Mater. Res, Part A* **2005**, *75A*, 810.
- [7] K. Bhattacharya, R. D. James, *Science* **2005**, *307*, 53.
- [8] Y. Bellouard, *Mater. Sci. Eng. A—Struct. Mater. Proper. Microstruct. Process.* **2008**, *481*, 582.
- [9] Y. Q. Fu, H. J. Du, W. M. Huang, S. Zhang, M. Hu, *Sens. Actuators, A* **2004**, *112*, 395.
- [10] P. Krulevitch, A. P. Lee, P. B. Ramsey, J. C. Trevino, J. Hamilton, M. A. Northrup, *J. Microelectromech. Syst.* **1996**, *5*, 270.
- [11] A. Ishida, M. Sato, *Acta Mater.* **2003**, *51*, 5571.
- [12] Y. Q. Fu, S. Zhang, M. J. Wu, W. M. Huang, H. J. Du, J. K. Luo, A. J. Flewitt, W. I. Milne, *Thin Solid Films* **2006**, *515*, 80.
- [13] M. Bouville, R. Ahluwalia, *Acta Mater.* **2008**, *56*, 3558.
- [14] T. Waitz, T. Antretter, F. D. Fischer, N. K. Simha, H. P. Karnthaler, *J. Mech. Phys. Solids* **2007**, *55*, 419.
- [15] T. Waitz, T. Antretter, F. D. Fischer, H. P. Karnthaler, *Mater. Sci. Technol.* **2008**, *24*, 934.
- [16] Y. Q. Fu, C. Shearwood, *Scr. Mater.* **2004**, *50*, 319.
- [17] C. P. Frick, T. W. Lang, K. Spark, K. Gall, *Acta Mater.* **2006**, *54*, 2223.
- [18] C. P. Frick, A. M. Ortega, J. Tyber, A. E. M. Maksound, H. J. Maier, Y. N. Liu, K. Gall, *Mater. Sci. Eng, A—Struct. Mater. Proper. Microstruct. Process.* **2005**, *405*, 34.
- [19] C. P. Frick, B. G. Clark, A. S. Schneider, R. Maaß, S. Van Petegem, H. Van Swygenhoven, *Scr. Mater.* **2010**, *62*, 492.
- [20] C. P. Frick, B. G. Clark, S. Orso, P. Sonnweber-Ribic, E. Arzt, *Scr. Mater.* **2008**, *59*, 7.
- [21] C. P. Frick, S. Orso, E. Arzt, *Acta Mater.* **2007**, *55*, 3845.
- [22] K. Gall, H. Sehitoglu, Y. I. Chumlyakov, I. V. Kireeva, H. J. Maier, *J. Eng. Mater. Technol. —Trans. ASME* **1999**, *121*, 19.
- [23] C. P. Frick, A. M. Ortega, J. Tyber, K. Gall, H. J. Maier, *Metall. Mater. Trans. A—Phys. Metall. Mater. Sci.* **2004**, *35A*, 2013.
- [24] C. A. Volkert, E. T. Lilleodden, *Philos. Mag.* **2006**, *86*, 5567.
- [25] C. Eberl, D. S. Gianola, R. Thompson, *Mathworks File Exchange Server* **2006**, File ID: 12413.
- [26] H. Zhang, B. E. Schuster, Q. Wei, K. T. Ramesh, *Scr. Mater.* **2006**, *54*, 181.
- [27] J. Ye, R. K. Mishra, A. R. Pelton, A. M. Minor, *Acta Mater.* **2010**, *58*, 490.
- [28] J. M. S. Juan, M. L. No, C. A. Schuh, *Adv. Mater.* **2008**, *20*, 272.
- [29] D. M. Dimiduk, M. D. Uchic, T. A. Parthasarathy, *Acta Mater.* **2005**, *53*, 4065.
- [30] C. P. Frick, B. G. Clark, S. Orso, A. S. Schneider, E. Arzt, *Mater. Sci. Eng, A—Struct. Mater. Proper. Microstruct. Process.* **2008**, *489*, 319.

- [31] T. A. Parthasarathy, S. I. Rao, D. M. Dimiduk, M. D. Uchic, D. R. Trinkle, *Scr. Mater.* **2007**, *56*, 313.
- [32] W. D. Nix, J. R. Greer, G. Feng, E. T. Lilleodden, *Thin Solid Films* **2007**, *515*, 3152.
- [33] K. Gall, H. Maier, *Acta Mater.* **2002**, *50*, 4643.
- [34] D. M. Norfleet, P. M. Sarosi, S. Manchiraju, M. F. X. Wagner, M. D. Uchic, P. M. Anderson, M. J. Mills, *Acta Mater.* **2009**, *57*, 3549.
- [35] K. Gall, H. Sehitoglu, Y. I. Chumlyakov, I. V. Kireeva, H. J. Maier, *J. Eng. Mater. Technol. –Trans. ASME* **1999**, *121*, 28.
- [36] O. Matsumoto, S. Miyazaki, K. Otsuka, H. Tamura, *Acta Metall.* **1987**, *35*, 2137.
- [37] B. Girault, A. S. Schneider, C. P. Frick, E. Arzt, *Adv. Eng. Mater.* **2010**, *12*, 385.
-